Electrochemically Reconstructed High-entropy Amorphous FeCoNiCrVB as A Highly active Oxygen Evolution Catalyst

Xu Zhong[1], Yin′an Zhu[1], Weiji Dai, Jin Yu, Tao Lu*, Ye Pan*

School of Materials Science and Engineering, Jiangsu Key Laboratory of Advanced

Metallic Materials, Southeast University, Nanjing 211189, China.

1. Xu Zhong and Yin′an Zhu contributed equally in this work.
*Correspondent Author: Ye Pan, e-mail: panye@seu.edu.cn
   Tao Lu, e-mail: lutao@seu.edu.cn
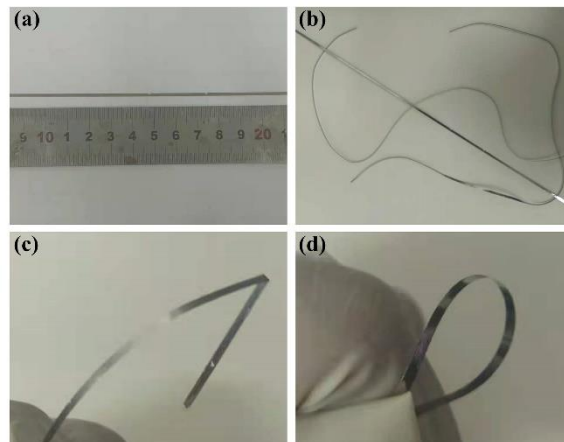
Fig S1. Photographs of robust p-FeCoNiCrVB as self-supported working electrodes
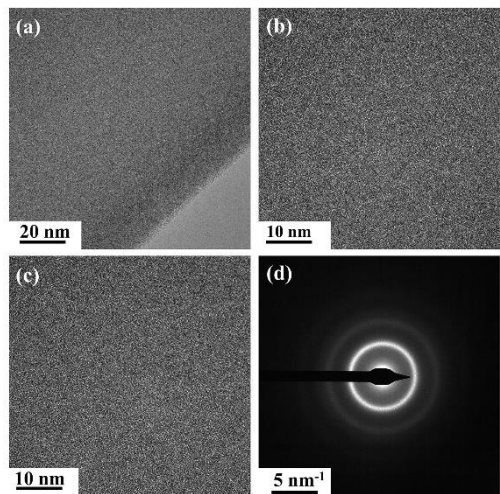
Fig S2. (a-c) HRTEM images of p-FeCoNiCrVB, (d) SAED pattern of p-FeCoNiCrVB
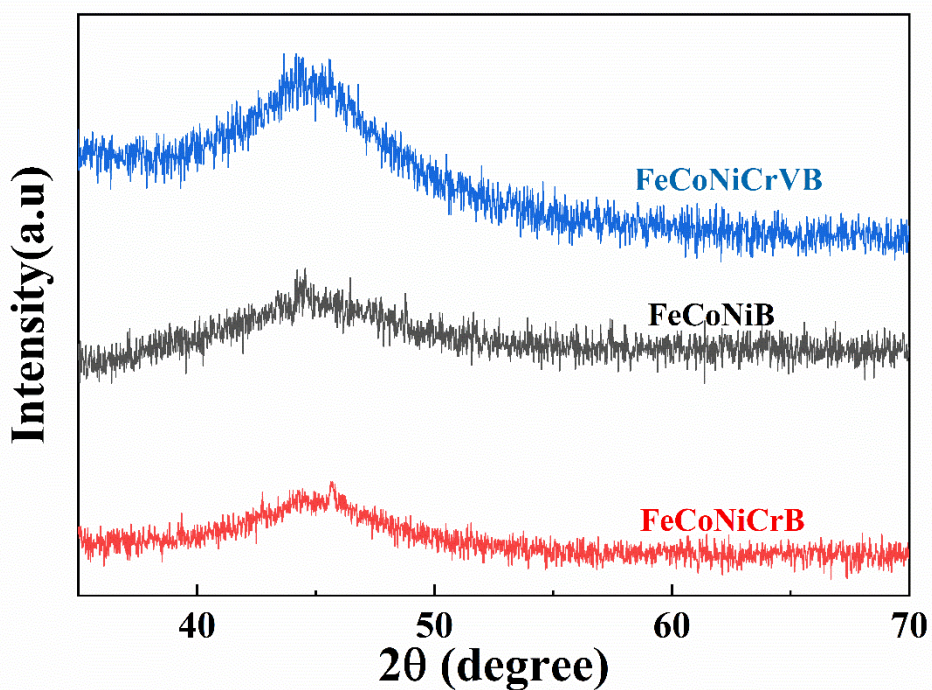

**Fig S3.** XRD patterns of p-FeCoNiB, p-FeCoNiCrB and p-FeCoNiCrVB
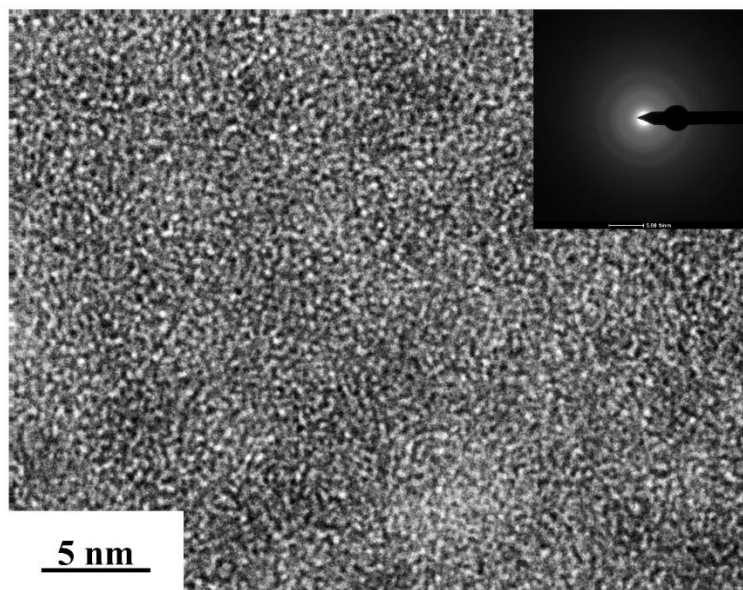
Fig S4. HRTEM image of surface layer of CV-FeCoNiCrVB (Inset is the corresponding SEAD pattern)
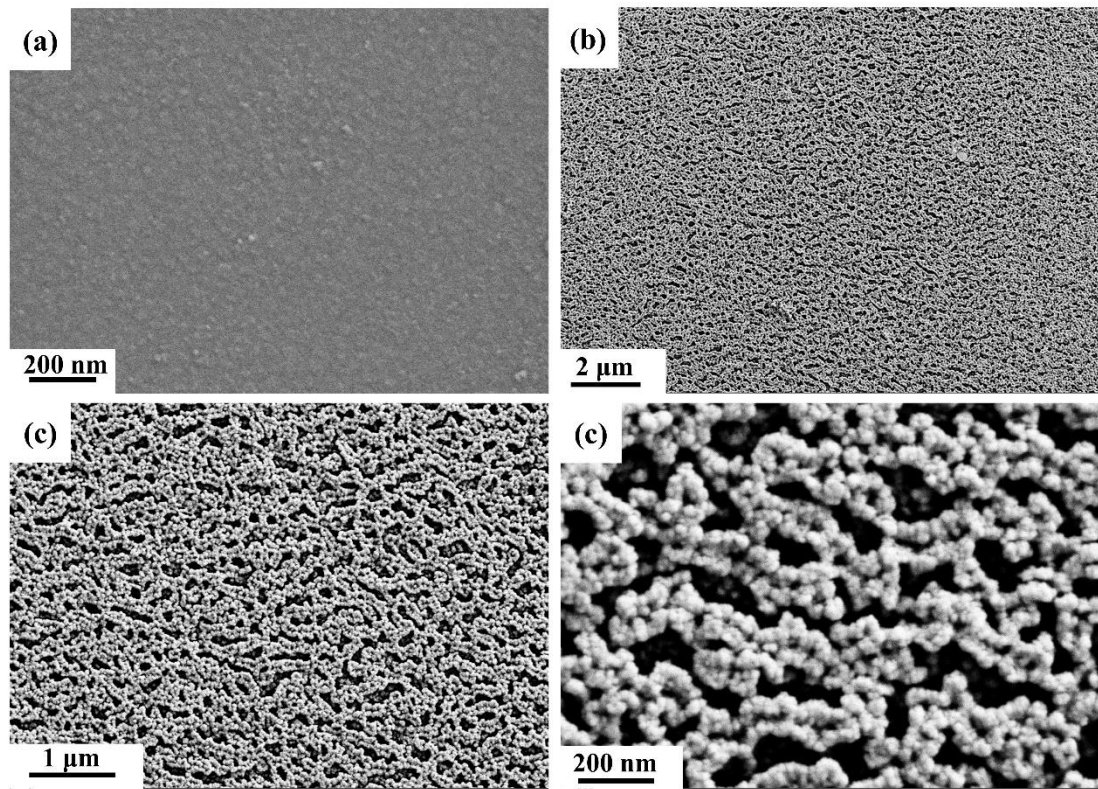
Fig S5. SEM images of (a) p-FeCoNiCrVB and (b-d) CV-FeCoNiCrVB
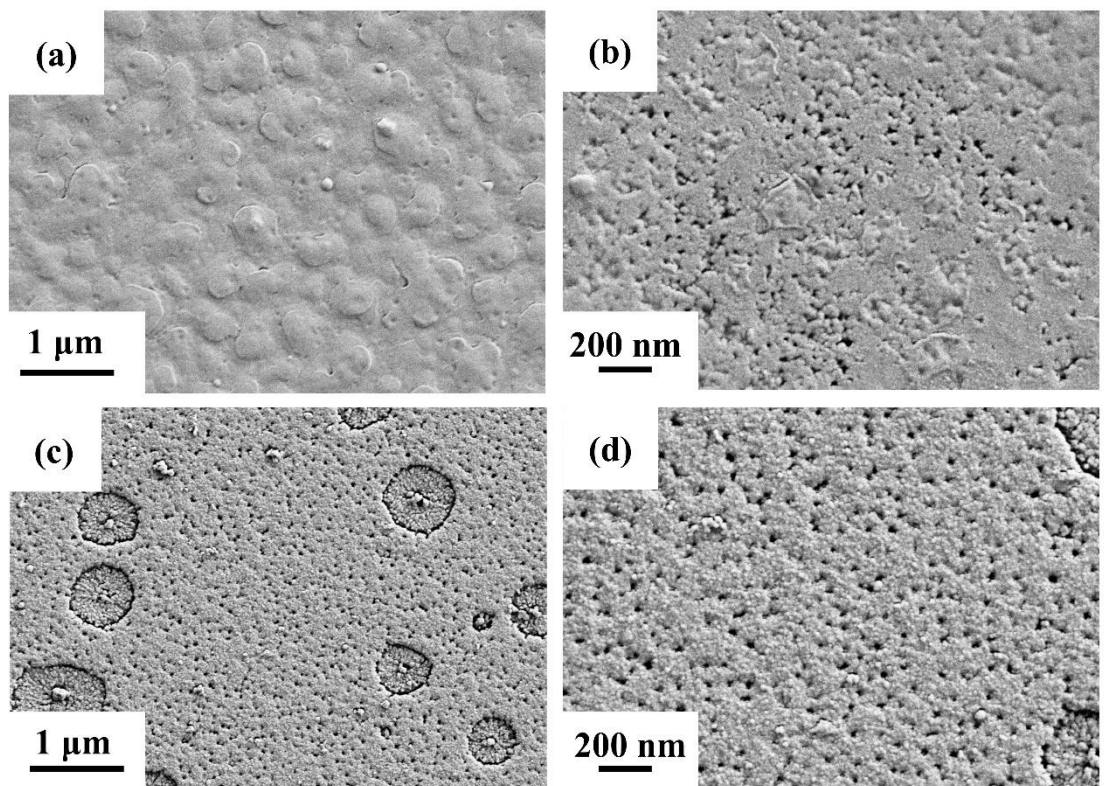
**Fig S6.** SEM images of (a, b) CV-FeCoNiB and (c, d) CV-FeCoNiCrB
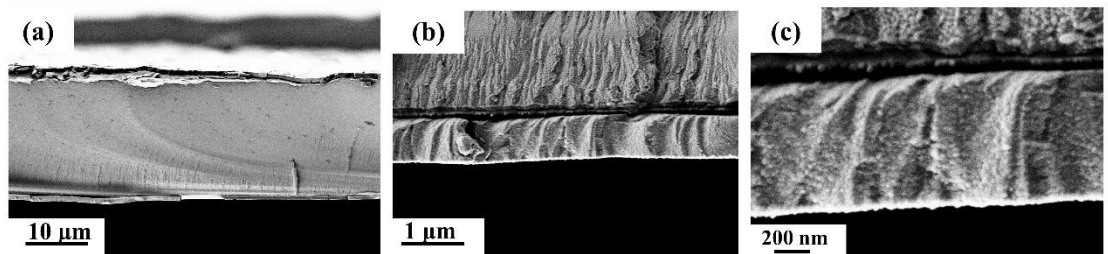
Fig S7. SEM images of section for CV-FeCoNiCrVB
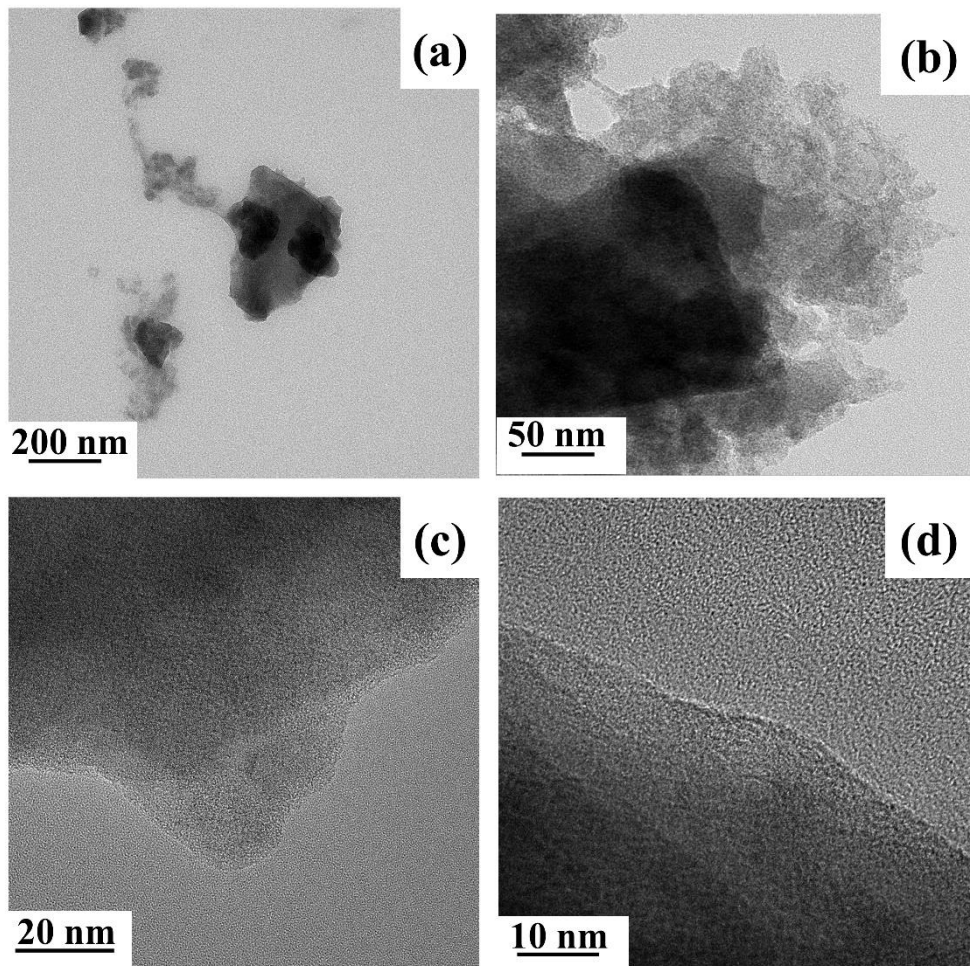
Fig S8. TEM images of core-shell structure of nanoparticles on surface of CV-FeCoNiCrVB
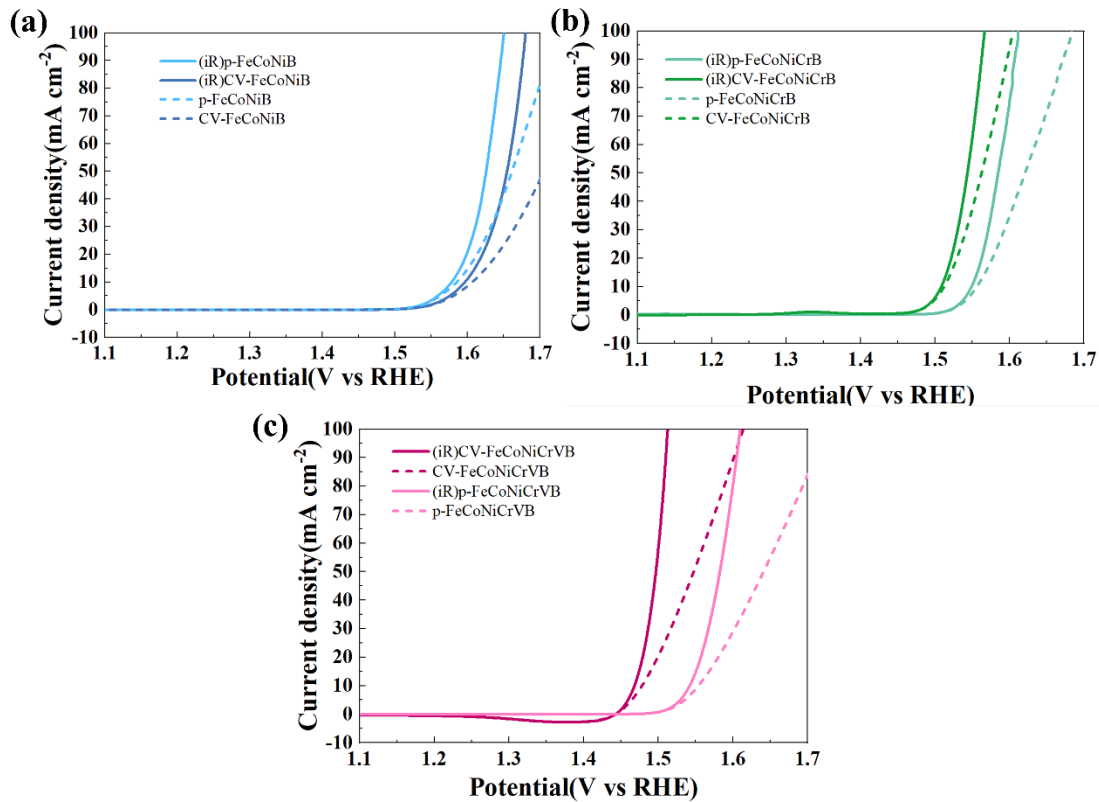
Fig S9. iR corrected LSV curves of (a)FeCoNiB, (b)FeCoNiCrB and (c)FeCoNiCrVB
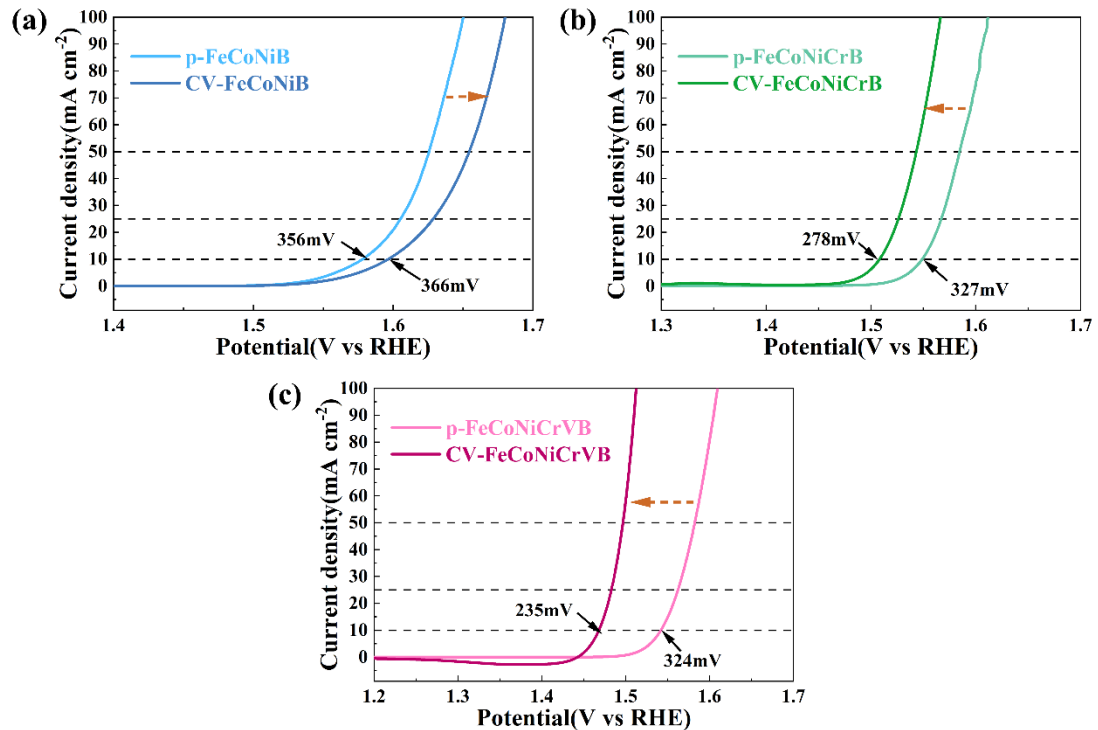
Fig S10. LSV curves of (a)FeCoNiB, (b)FeCoNiCrB and (c)FeCoNiCrVB before and after CV activation.
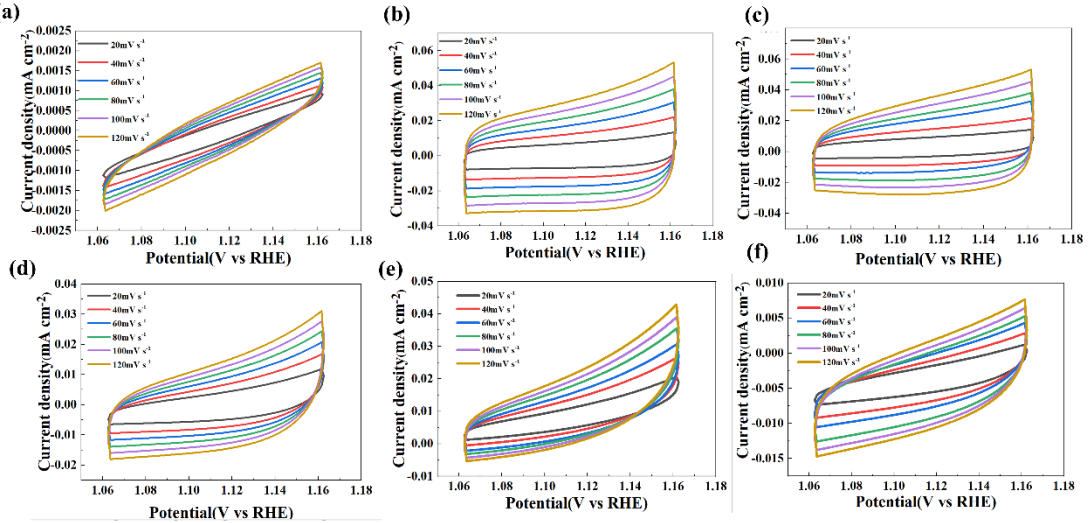
Fig S11. CV curves of (a) p-FeCoNiB, (b) CV-FeCoNiB, (c) p-FeCoNiCrB, (d) CV-FeCoNiCrB, (e) p-FeCoNiCrVB, and (f) CV-FeCoNiCrVB at scan rates ranging from 20 mV s^{-1} to 120 mV s^{-1} with an interval point of 20 mV s^{-1}
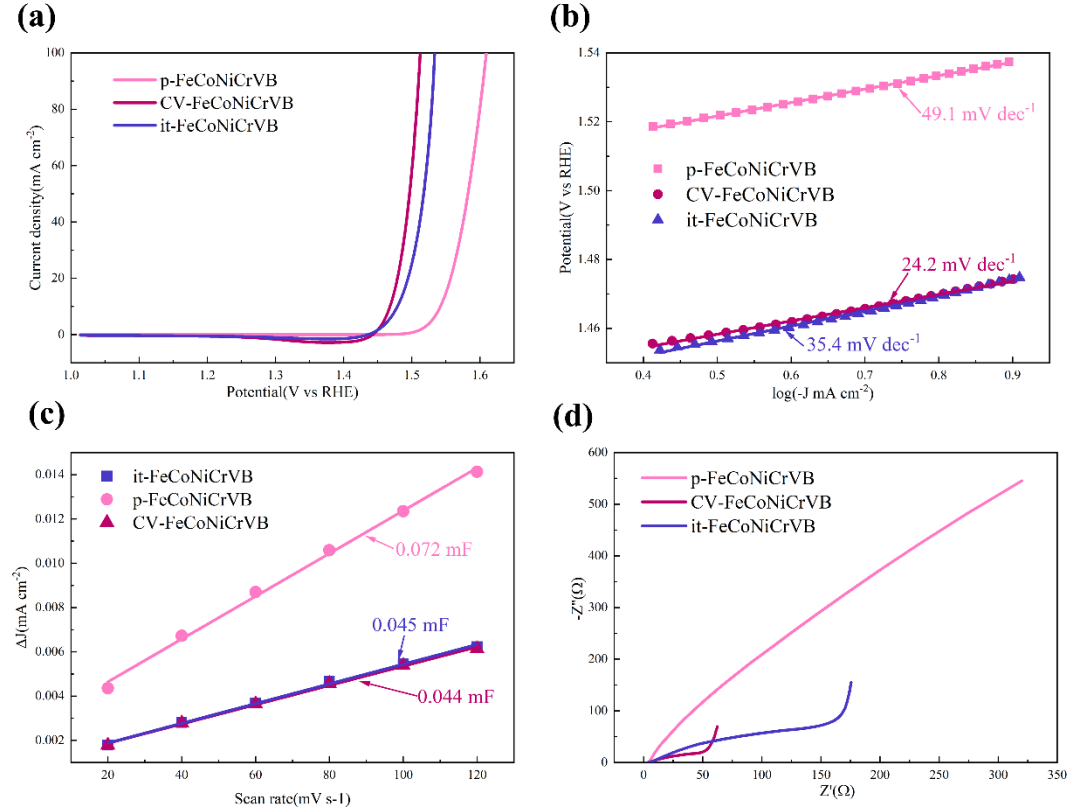
Fig S12. (a) LSV curves, (b)Tafel slopes, (c)ECSA, (d)EIS of p-FeCoNiCrVB, CV-FeCoNiCrVB and it-FeCoNiCrVB.
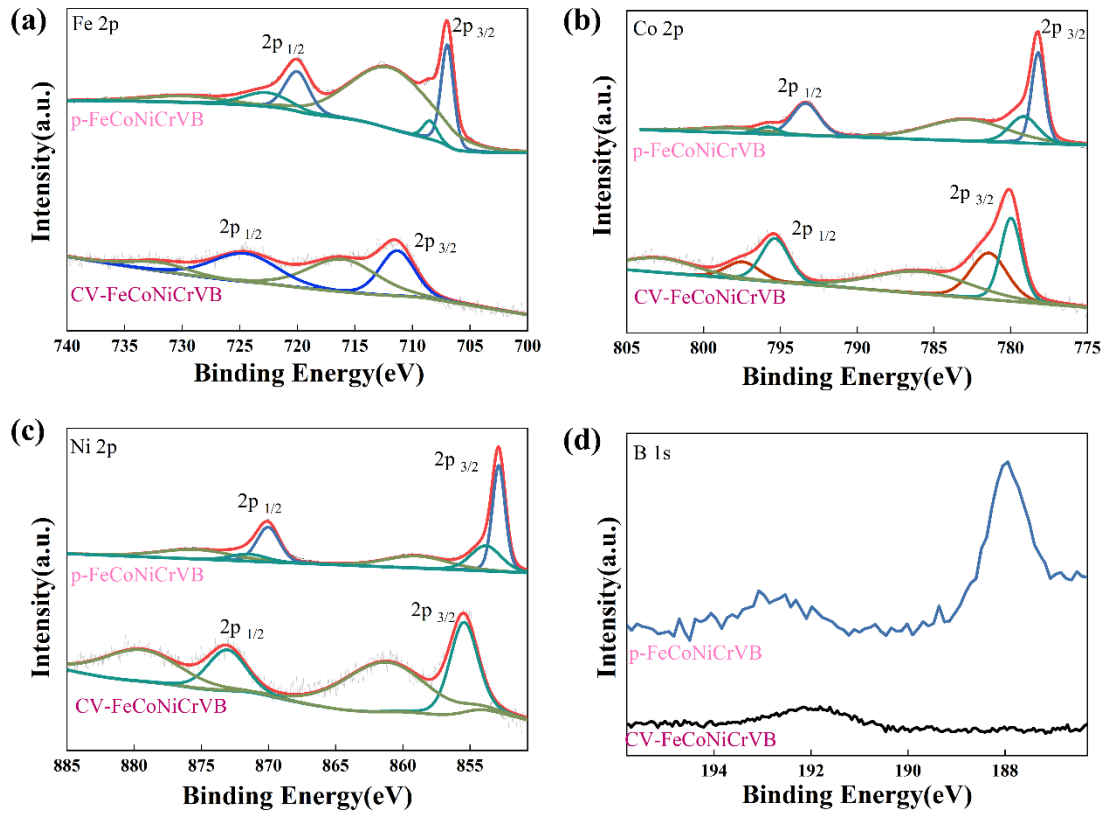
Fig S13. XPS of (a) Fe 2p, (b) Co 2p, (c) Ni 2p and (d) B 1s of p-FeCoNiCrVB and CV-FeCoNiCrVB.

In the Fe 2p spectra of p-FeCoNiCrVB(Fig S13a), the peaks at 706.9eV (Fe 2p3/2) and 720.1eV (Fe 2p1/2) are attributed to the presence of Fe^0, and the peaks around 708.7(2p 3/2) and 722.9(2p 1/2) belong to Fe^{2+}. From Co 2p spectra of p-FeCoNiCrVB (Fig S13b), the Co 2p3/2 are deconvoluted into two peaks at 778.2eV (Co^0) and 779.2eV (Co^{2+}), Co 2p1/2 peaks are located at 793.3(Co^0) and 795.9 eV (Co^{2+}), respectively. Ni 2p spectra of p-FeCoNiCrVB (Fig S13c) have peaks at 852.9eV (Ni 2p3/2) and 870.1eV (Ni 2p1/2) of Ni^0, and peaks at around 854.1 (Ni 2p3/2) and 871.5 (Ni 2p1/2) eV of Ni^{2+}. XPS spectrums of Fe, Co and Ni before activation clearly specify dominant existence of metallic phases.

For the Fe 2p spectrum of CV-FeCoNiCrVB(Fig S13a), two peaks located at 711.3eV and 724.7eV could be attributed to Fe^{3+}. The Co 2p spectrum of CV-FeCoNiCrVB (Fig S13b) could be fitted into Co^{2+}(779.9eV and 795.4eV) and Co^{3+}(781.7eV and 797.5eV), respectively. In the Ni 2p spectrum (Fig S13c), the peaks at 855.5eV and 873.2eV are identified with the signals of Ni^{2+}. Apparently, the Fe/Co

/Ni species are oxidized or hydroxylated gradually, and the metallic phases for elements totally vanished after CV activation. Increasing extent of high-valence Fe/Co/Ni species and existence of divalent and trivalent states, signifying greater possibility for enhancement of catalytic performance.

The B 1s spectrum of p-FeCoNiCrVB are deconvoluted into two distinct peaks at 187.8eV and 192.2eV. (Fig S13d) The peak at 187.07eV is due to B^0, whereas the one at 192.2eV is due to boron-oxo species. Differently, the B 1s spectrum of CV-FeCoNiCrVB at 191.9eV corresponds to boron oxide species. The peak ascribed to B^0 is hard to be detected, due to the CV activation process. A negative shift of boron oxide species between pristine and activated one, are indicative of the electron transfer towards boron elements from metal elements[1]. It is reported that the electron transfer from metalloid element to metal elements could weaken bonds among metal atoms and further induce rearrangement of the electron density around the catalytic metal atom center[2,3].
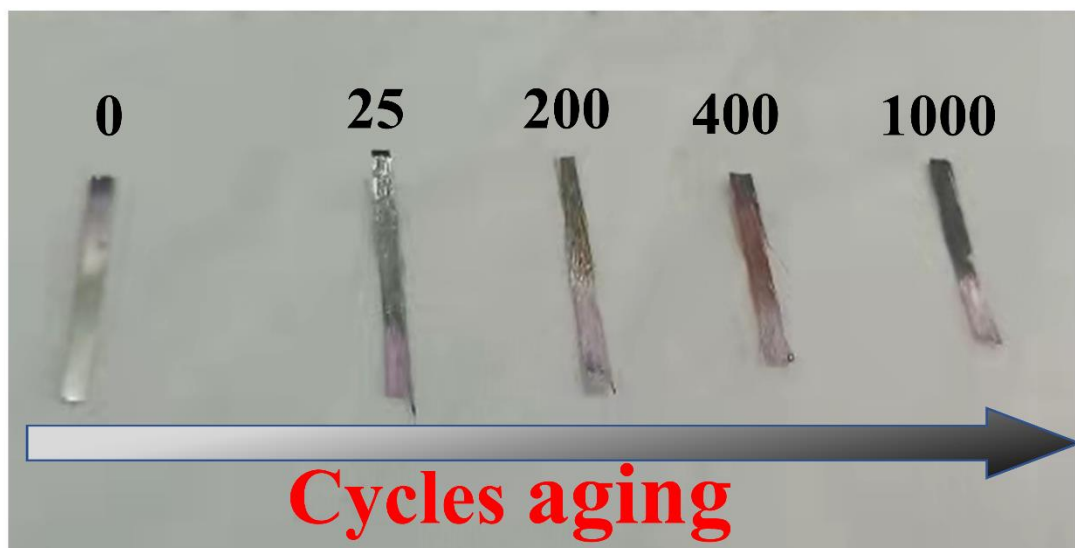

Fig S14. Color transition with cycles aging for FeCoNiCrVB
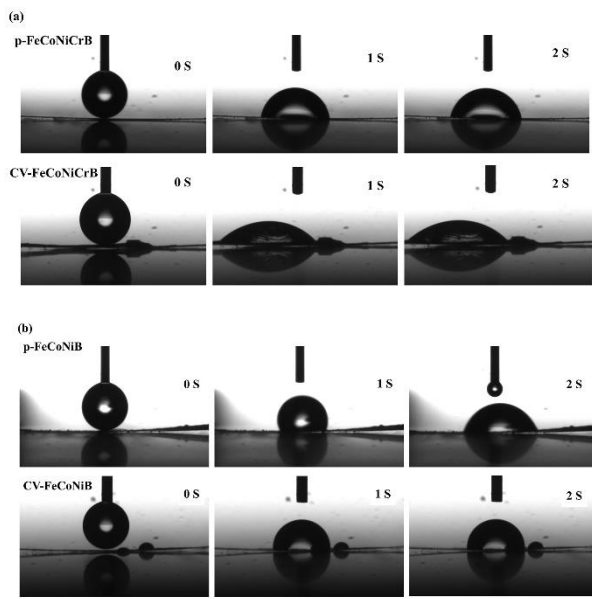
Fig S15. Contact angles of (a) FeCoNiCrB and (b) FeCoNiB
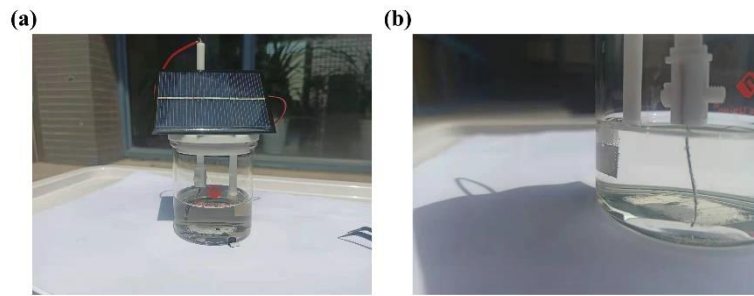
Fig S16. Photographs of (a) the overall water splitting driven by a solar cell, (b) two electrodes device for water spitting in 1 M KOH.

Table S1. Summary of high-entropic materials as OER catalysts

Catalysts	Overpotential(mV)To reach 10 mA cm^{-2}	Tafel slopes (mV dec^{-1})	Reference
CV-FeCoNiCrVB	237	24.2	This work
p-FeCoNiCrVB	311	49.1	This work
CV-FeCoNiCrB	278	46.5	This work
p-FeCoNiCrB	319	47.8	This work
CV-FeCoNiB	367	63.5	This work
p-FeCoNiB	348	55.7	This work
MnFeCoNiCu	263	43	[4]
FeCoNiCrNb	288	27.7	[5]
AlNiCoIrMo	233	55.2	[6]
(CoCuFeMnNi)$_3$O$_4$	350	58.5	[7]
CoCrFeMnNiP$_x$	320	60.8	[8]
KNa(MgMnFeCoNi)F$_3$	369	61	[9]
NiCoFeMnCrP	270	52.5	[10]
(CoNiMnZnFe)$_3$O$_{3.2}$	336	47.5	[11]
AlAgAuCoCuFeIrMoRuNiPdPtRhTi	258	84.2	[12]

Table S2. Summary of OER catalysts containing boron

Catalysts	Overpotential(mV)To reach 10 mA cm^{-2}	Tafel slopes (mV dec^{-1})	Reference
CV-FeCoNiCrVB	237	24.2	This work
p-FeCoNiCrVB	311	49.1	This work
CV-FeCoNiCrB	278	46.5	This work
p-FeCoNiCrB	319	47.8	This work
CV-FeCoNiB	367	63.5	This work
p-FeCoNiB	348	55.7	This work
RuO$_2$	305	91.5	This work
Fe-Co-Ni-B	274	38	[13]
Ni$_x$–B nanosheets	380	89	[14]
Co-Fe-B	298	62.6	[15]
Co-Ni-B	310	66	[16]
V-doped Co-Ni boride	280	101	[16]
Ni-B	360	76	[17]
Co-B	340	63	[18]
Co$_3$B	312	53	[19]
Co$_2$B	380	45	[20]
FeB$_2$	296	52.4	[21]

Table S3. Selected standard reduction potentials versus standard hydrogen electrode (SHE) of metals

Reduction half Reaction	Standard Reduction Potential(V vs SHE)
$V^{3+}(aq)+3e^-\rightarrow V(s)$	-1.175
$Cr^{3+}(aq)+3e^-\rightarrow Cr(s)$	-0.744
$Fe^{2+}(aq)+2e^-\rightarrow Fe(s)$	-0.447
$Co^{2+}(aq)+2e^-\rightarrow Co(s)$	-0.28
$Ni^{2+}(aq)+2e^-\rightarrow Ni(s)$	-0.257

Selected Standard Reduction Potentials at 25℃

Reference:

1   C. F. Li, J. W. Zhao, L. J. Xie, J. Q. Wu and G. R. Li, *Appl. Catal. B Environ.*, 2021, **291**, 119987.

2   A. Sivanantham, P. Ganesan, A. Vinu and S. Shanmugam, *ACS Catal.*, 2020, **10**, 463–493.

3   Z. Qiu, C. W. Tai, G. A. Niklasson and T. Edvinsson, *Energy Environ. Sci.*, 2019, **12**, 572–581.

4   K. Huang, B. Zhang, J. Wu, T. Zhang, D. Peng, X. Cao, Z. Zhang, Z. Li and Y. Huang, *J. Mater. Chem. A*, 2020, **8**, 11938–11947.

5   Z. Ding, J. Bian, S. Shuang, X. Liu, Y. Hu, C. Sun and Y. Yang, *Adv. Sustain. Syst.*, 2020, **4**, 1–9.

6   Z. Jin, J. Lv, H. Jia, W. Liu, H. Li, Z. Chen, X. Lin, G. Xie, X. Liu, S. Sun and H. J. Qiu, *Small*, 2019, **15**, 1–7.

7   D. Wang, Z. Liu, S. Du, Y. Zhang, H. Li, Z. Xiao, W. Chen, R. Chen, Y. Wang, Y. Zou and S. Wang, *J. Mater. Chem. A*, 2019, **7**, 24211–24216.

8   X. Zhao, Z. Xue, W. Chen, Y. Wang and T. Mu, *ChemSusChem*, 2020, **13**, 2038–2042.

9   T. Wang, H. Chen, Z. Yang, J. Liang and S. Dai, *J. Am. Chem. Soc.*, 2020, **142**, 4550–4554.

10 D. Lai, Q. Kang, F. Gao and Q. Lu, *J. Mater. Chem. A*, 2021, **9**, 17913–17922.

11 Y. Zhang, W. Dai, P. Zhang, T. Lu and Y. Pan, *J. Alloys Compd.*, 2021, **868**, 159064.

12 Z. X. Cai, H. Goou, Y. Ito, T. Tokunaga, M. Miyauchi, H. Abe and T. Fujita, *Chem. Sci.*, 2021, **12**, 11306–11315.

13 J. M. V. Nsanzimana, Y. Peng, Y. Y. Xu, L. Thia, C. Wang, B. Y. Xia and X. Wang, *Adv. Energy Mater.*, 2018, **8**, 1–7.

14 J. Masa, I. Sinev, H. Mistry, E. Ventosa, M. de la Mata, J. Arbiol, M. Muhler, B. Roldan Cuenya and W. Schuhmann, *Adv. Energy Mater.*, 2017, 7.

15 H. Chen, S. Ouyang, M. Zhao, Y. Li and J. Ye, *ACS Appl. Mater. Interfaces*, 2017, **9**, 40333–40343.

16 J. Zhang, X. Li, Y. Liu, Z. Zeng, X. Cheng, Y. Wang, W. Tu and M. Pan, *Nanoscale*, 2018, **10**, 11997–12002.

17 H. S. Han, Y. R. Hong, J. Woo, S. Mhin, K. M. Kim, J. Kwon, H. Choi, Y. C. Chung and T. Song, *Adv. Energy Mater.*, 2019, **9**, 1–11.

18 Y. Liang, X. Sun, A. M. Asiri and Y. He, *Nanotechnology*, , DOI:10.1088/0957-4484/27/12/12LT01.

19 X. Ma, J. Wen, S. Zhang, H. Yuan, K. Li, F. Yan, X. Zhang and Y. Chen, *ACS Sustain. Chem. Eng.*, 2017, **5**, 10266–10274.

20 J. Masa, P. Weide, D. Peeters, I. Sinev, W. Xia, Z. Sun, C. Somsen, M. Muhler and W. Schuhmann, *Adv. Energy Mater.*, 2016, **6**, 1–10.

21 H. Li, P. Wen, Q. Li, C. Dun, J. Xing, C. Lu, S. Adhikari, L. Jiang, D. L. Carroll and S. M. Geyer, *Adv. Energy Mater.*, 2017, **7**, 1–12.